Frontiers in Bioscience Landmark

Front. Biosci. (Landmark Ed) **2024**; 29(3): 98
https://doi.org/10.31083/j.fbl2903098

Original Research

Prognostic Model Associated with Necroptosis in Colorectal Cancer based on Transcriptomic Analysis and Experimental Validation

Yuying Huang[1,2,†], Licheng Li[3,†], Zhongmin Kang[3,4], Huali Luo[2], Xiaojing Lin[1], Shu Zhao[1,5], Qizhu Zhang[1], Qinshan Li[1,2,*], Honglin Liu[6,*], Mengxing Li[3,4,7,*]

[1]Institute of Precision Medicine of Guizhou Province, Department of Obstetrics and Gynecology, Affiliated Hospital of Guizhou Medical University, 550004 Guiyang, Guizhou, China
[2]Department of Clinical Biochemistry, School of Medical Laboratory Science, Guizhou Medical University, 550004 Guiyang, Guizhou, China
[3]Clinical Medical College, Guizhou Medical University, 550004 Guiyang, Guizhou, China
[4]Department of Hematology, Affiliated Hospital of Guizhou Medical University, Guizhou Province Institute of Hematology, Guizhou Province Laboratory of Hematopoietic Stem Cell Transplantation Centre, 550004 Guiyang, Guizhou, China
[5]Department of Obstetrics, Guizhou Provincial People's Hospital, 550499 Guiyang, Guizhou, China
[6]Institute of Clinical Medical Sciences, China-Japan Friendship Hospital, 100000 Beijing, China
[7]Department of Pathophysiology, Guizhou Medical University, 550004 Guiyang, Guizhou, China
*Correspondence: liqinshan@gmc.edu.cn (Qinshan Li); honglinl2003@163.com (Honglin Liu); lmx1234@gmc.edu.cn (Mengxing Li)
[†]These authors contributed equally.

Academic Editor: Elisa Belluzzi
Submitted: 10 November 2023 Revised: 26 December 2023 Accepted: 29 December 2023 Published: 11 March 2024

Abstract

Purpose: Numerous studies have emphasised the importance of necroptosis in the malignant progression of colorectal cancer (CRC). However, whether necroptosis-related genes (NRGs) can be used to predict the prognosis of CRC remains to be revealed. **Methods**: Patients with CRC were divided into two clusters based on the expression of NRGs, and prognosis was compared between the two clusters. A prognostic model was established based on NRGs, and its predictive efficiency was validated using Kaplan-Meier (K-M) curves, receiver operating characteristic (ROC) curves and a nomogram. Immune infiltration, single-cell and drug sensitivity analyses were used to examine the effects of NRGs on the prognosis of CRC. **Results**: The prognostic model served as a valid and independent predictor of CRC prognosis. Immune infiltration and single-cell analyses revealed that the unique immune microenvironment of CRC was regulated by NRGs. Drug sensitivity analysis showed that patients in the high- and low-risk groups were sensitive to different drugs. In addition, *H2BC18* was found to play an important role in regulating the malignant progression of CRC. **Conclusion**: This study provides novel insights into precision immunotherapy based on NRGs in CRC. The NRG-based prognostic model may help to identify targeted drugs and develop more effective and individualised treatment strategies for patients with CRC.

Keywords: necroptosis; colorectal cancer; prognostic model; TCGA; immune infiltration

1. Introduction

Colorectal cancer (CRC) is a prevalent malignant gastrointestinal tumour worldwide. According to global cancer statistics, approximately 1.4 million new cases of CRC were reported in 2020, with CRC accounting for 9.4% of all cancer-related deaths [1]. Although remarkable advancements have been made in the prevention, screening and treatment of CRC in the past decade, the death rate of patients with CRC remains high [2], with the 5-year survival rate of patients with metastatic CRC being only 12% [3]. The main causes of recurrence and death in patients with CRC are local tumour infiltration, distant metastasis and resistance to existing therapies. Therefore, effective prognostic biomarkers should be identified and accurate prognostic models should be developed to reduce the risk of recurrence and death in patients with CRC. Necroptosis, first proposed by Degterev *et al.* [4] in 2005, is a novel cell death mechanism that relies on mixed lineage kinase domain-like proteins (MLKL/PMLKL) activated by receptor-interacting protein kinase-1/3 (RIPK1/RIPK3). Numerous studies have shown that necroptosis plays a crucial role in promoting and inhibiting cancer development [5–7]. However, to date, most studies on CRC have focused on the anti-tumour effects of typical necroptosis-related genes (NRGs) such as *RIPK1/RIPK3* and *MLKL/PMLKL*. For example, Han *et al.* [8] found that resorcytoxin inhibited tumour growth by inducing necroptosis in CRC cells through an *RIPK3*-mediated mechanism and that *GDC-0326* enhanced the anti-tumour effects of the chemotherapeutic drug 5-fluorouracil (5-Fu) by inducing necroptosis [9]. With regard to the tumour-specific effects of NRGs on CRC, Wang *et al.* [10] found that *RIPK1*, *RIPK3* and *MLKL* genes were significantly upregulated and promoted the proliferation of cancer cells in mice with CRC treated with radiation therapy. Given that the role of necroptosis in CRC remains unclear, the effects of NRGs on the prognosis of CRC should be further investigated to elucidate the potential molecular mechanisms and regulatory networks.

In this study, we investigated differentially expressed NRGs between CRC and adjacent normal tissues in The Cancer Genome Atlas (TCGA) datasets and identified two molecular subtypes of CRC using unsupervised clustering. Subsequently, the expression patterns of NRGs, enriched pathways, tumour microenvironment (TME) characteristics and prognosis were compared between the two subtypes. A prognostic risk model based on four NRGs, namely, *GABPB1-IT1*, *H2BC18*, *HSPA1L* and *MIR503HG*, was constructed using LASSO–Cox regression, and its predictive accuracy was evaluated using Kaplan-Meier (K-M) curves, receiver operating characteristic (ROC) curves and a nomogram. Immune infiltration analysis showed that the expression of the four NRGs was markedly associated with the abundance of activated NK cells and $CD4^+$ memory T cells. Drug sensitivity analysis indicated that oral PARP inhibitors had better sensitivity in the high-risk group, whereas LCK inhibitors, third-generation AKT inhibitors, JNK inhibitors and the third-generation ABL inhibitor ponatinib were potentially efficacious in the low-risk group. Finally, single-cell analysis showed that *HSPA1L* was highly expressed in fibroblasts and endothelial cells, whereas was highly expressed in epithelial cells, suggesting that the unique immune microenvironment of CRC was regulated by NRGs. The results of this study collectively suggest that the NRG-based risk model is a valid and independent predictor of CRC prognosis and may help to characterise the immune microenvironment of CRC and develop potential targeted therapies. Altogether, this study proposes a novel approach to diagnosing CRC and predicting its prognosis in clinical settings.

2. Materials and Methods

2.1 Data Collection and Collation

We downloaded the RNA-sequencing and clinical data of 328 tissue samples, including 40 adjacent normal tissues and 288 CRC tissues, from The Cancer Genome Atlas (TCGA) database (https://www.cancer.gov/ccg/research/genome-sequencing/tcga). The robust multi-array averaging (RMA) algorithm in the 'affy' R package (version 1.46.1) [11] was used to process these data. In addition, batch effects were removed using the 'sva' R package (version 3.42.0) [12]. Differentially expressed genes (DEGs) between CRC and normal tissues were identified using the 'limma' R package (version 3.42.2) [13], with the screening criteria set as |logFC| values of $\geq$1 (FC: fold change) and corrected *p*-values of $<$0.05. NRGs were collected from the GeneCards database (https://www.genecards.org/), and a Venn diagram was generated to represent the intersection between DEGs and NRGs. Genes with correlation coefficients of $>$0.2 were used for subsequent analysis.

2.2 Consensus Clustering of NRGs

The 'ConensusClusterPlus' R package (version 1.66.0) was used for consensus clustering analysis of NRGs [14]. Based on the expression of NRGs, two molecular subtypes were generated through K-means clustering. Gene set variation analysis (GSVA) was performed on gene sets extracted from MSigDB (C2.Cp.ke.v7.2) [15] to examine differences in biological functions between the two molecular subtypes.

2.3 Comprehensive Analysis of the Two Molecular Subtypes

We compared the prognosis and clinical features of patients with CRC between the two molecular subtypes. To compare overall survival (OS) between the two subtypes, Kaplan-Meier curves were generated using the 'survival' and 'survminer' R packages (version 4.2.3). The CIBERSORT algorithm was used to estimate the immune scores of 22 immune cell types in each CRC sample based on cell-specific gene signatures [16].

2.4 Construction of an NRG-related Prognostic Model

The 'limma' R package (version 3.42.2) was used to screen for DEGs between the two molecular subtypes [13], with the screening criteria set as |logFC| values of $\geq$1 and adjusted *p*-values of $<$0.05. Patients with CRC were randomly assigned to training (n = 287) and test (n = 41) sets, which were used to develop a prognostic risk model [17]. Lasso–Cox regression analysis was implemented to reduce the risk of overfitting and to establish a risk model based on prognosis-associated NRGs. The prognostic NRG-Score was calculated based on the risk model as follows [18]: $\sum_i^n Coefi \times Ai$. In the aforementioned equation, Coefi represents the risk coefficient and Expi represents the expression of the gene. The training and test sets were divided into high- and low-risk groups based on the median NRG-Score. Kaplan-Meier and receiver operating characteristic (ROC) curves were plotted to evaluate the generalisability and predictive accuracy of the model.

2.5 Development of a Predictive Nomogram

The 'RMS' package (version 3.6.1) was used to establish a predictive nomogram based on NRG-Scores and clinical characteristics of CRC [19]. Column charts demonstrating NRG-Scores and predicted OS rates were generated, and calibration curves were plotted to compare the predicted and actual 1-, 3- and 5-year OS rates [20].

2.6 Combined Analysis of Molecular and Immune Characterisation of NRG-score

The infiltration levels of 22 types of immune cells were evaluated based on the expression of the four prognostic NRGs included in the risk model (model genes). A boxplot was generated to compare the expression of immune checkpoint genes between the low- and high-risk groups. In addition, drug sensitivity was compared between the two risk groups. The 'pRRophetic' package (version 4.3.2) was

used to calculate the half-maximal inhibitory concentration (IC50) of targeted drugs to evaluate their clinical efficacy in the two risk groups [21].

2.7 Distribution of Model Genes at the Single-cell Level

The 'Seurat' package (version 5.0.1) was used to generate a Seurat object and remove poor-quality cells. A standard procedure was used to pre-process the data, and the percentages of gene count, cell count and mitochondrial content were subsequently calculated. Cells with $<$200 or $>$6000 genes and with $>$5% of transcripts derived from mitochondria were excluded. To normalise the data of each cell, UMI counts were scaled using a scale factor of 10,000. After the logarithmic transformation of the data, the ScaleData function was used to analyse corrected normalised data metrics. Principal component analysis (PCA) was performed using the top 10 variable genes, and the top 5 principal components were visualised and clustered via UMAP (or TSNE). Cells were clustered using the FindClusters function implemented in the Seurat R package.

2.8 Cell Culture and Transfection

The human CRC cell lines HCT116, HT29 and HCT15 and the normal human colorectal epithelial cell line NCM460 were purchased from the Cell Center of the Institute of Basic Medical Sciences, Chinese Academy of Medical Sciences. All cells were cultured in DMEM (Gibco, New York, NY, USA) supplemented with 10% foetal bovine serum (FBS) (VivaCell, Shanghai, China) and 1% penicillin-streptomycin (Gibco, New York, NY, USA) in a humidified environment with 5% CO_2 at 37 ℃. The cells were transfected with siRNAs using Lipo8000TM transfection reagent (Biyuntian, Shanghai, China) according to the instruction manual. All cell lines were validated by short tandem repeat (STR) profiling and tested negative for mycoplasma. The target sequences of *H2BC18* siRNA were shown in Table 1.

Table 1. Three target sequences of H2BC1 small interfering RNA (siRNA).

si*H2BC18*-242	AAGAUGUCGUUGACGAAGGAGTT
si*H2BC18*-104	UUCUUCUGCACUUUCGUAACATT
si*H2BC18*-410	UACUUCGAGCUGGUGUACUUGTT

2.9 Quantitative Reverse Transcription Polymerase Chain Reaction

For quantitative reverse transcription polymerase chain reaction (qRT-PCR), total RNA was extracted from CRC cells using Trizol reagent (Takara, Kyoto, Japan) and was reverse transcribed using Prime Script RT Master Mix (Takara, Kyoto, Japan). Quantitative PCR (qPCR) was performed using total 2 µL of mRNA, specific primers and SYBR Premix Ex Taq II (Takara, Kyoto, Japan). The mRNA expression of target genes was normalised to that of GAPDH (internal control) and quantified using the $2^{-\Delta\Delta Ct}$ method [22]. Primers were synthesised by Sangon Biotech (Sangon, Shanghai, China). The gene-specific primers sequences were shown in Table 2.

2.10 Cell Counting Kit-8 (CCK-8) Assay

The cells were digested utilising 0.25% trypsin and centrifuged at a speed of 1200 rpm/min for 5 min. The supernatant was discarded, and the cell precipitate was resuspended in 1 mL of a complete medium. Subsequently, the cells were counted using a Bovine Bow counting plate (QiuJing, Shanghai, China) with a filled cell. The cell suspension was diluted to a concentration of 1×10^3 cells/well, and 200 µL of the cell suspension was added to each well of a 96-well plate. The cells were maintained in an incubator, and the original medium was replaced with 100 µL of a serum-free medium containing 10% CCK-8 reagent on days 0, 1 and 2. The CCK-8-treated cells were then incubated at 37 ℃ for two hours. Following this, the optical density (OD) of every well was measured using an enzyme marker (MCE, South Brunswick Township, NJ, USA) at 450 nm.

2.11 Migration, Invasion and Wound Healing Assays

Migration assay: Cells were cultured in a serum-free medium overnight. The following day, the cells were digested using 0.25% trypsin and centrifuged at 1200 rpm/min for 5 min. The supernatant was discarded, and the cell precipitate was washed thrice with PBS. The cells were resuspended in 1 mL of a basal medium and counted on Oxbow counting plates. The concentration of HCT15 cells was adjusted to 4×10^4 cells/well. A total of 600 µL of a medium containing 10% FBS was added to a 24-well plate serving as the lower chamber, and a Transwell insert serving as the upper chamber was placed into the plate. HCT15 cells were added to the upper chamber (200 µL/well) and cultured routinely for 48 h. After the media in the Transwell chamber and plate were discarded, the migrated cells were washed twice with PBS, fixed with 4% paraformaldehyde for 30 min and stained with crystal violet for 15 min. A moistened cotton swab was used to gently remove the cells from the upper chamber. Thereafter, the cells were photographed using a Nikon eclipse80i confocal fluorescence microscope (Nikon, Tokyo, Japan).

Invasion assay: The basal medium was used to dilute a substrate gel at a ratio of 1:8. A total of 60 µL of the diluted gel was added to the chambers, followed by incubation at 37 °C for 2 h. The subsequent steps were the same as those for the migration assay.

Wound healing assay: CRC cells were cultured in 6-well plates until $\geq$90% confluence was achieved. The surface of the cell monolayer in each well was scratched with a sterile 200-µL pipette tip. Floating cells were washed with PBS, and a serum-free medium was added to each well. Photographs were captured at 0 h, 48 h and 72 h af-

Table 2. Gene-specific primers for qRT-PCR.

Gene	Forward (5′-3′)	Reverse (5′-3′)
CDKN2A	AGACTTTCGAAGAGGGGGAGCC	GCCCATCATCATGACCAGGAACA
GABPB1-IT1	AACCTGATTGGACTGTGGCG	GAGAGCAAAACAGTCCGGAGA
H2BC18	CCAAGTACACCAGCTCGAAGTTA	GTTGATGGGCAAGTGGGGTGA
MIR503HG	AAGGAATCCTCTCCCACCATTT	ACTCATTTGGCGGGAAAAC
GAPDH	CGGAGTCAACGGATTTGGTCGTAT	AGCCTTCTCCATGGTGG TGAAGAC

qRT-PCR, quantitative reverse transcription polymerase chain reaction.

ter the scratches were made, and changes in the area of the scratches were quantified using the ImageJ software (Image J2x 2.1.5.0, National Institutes of Health, New York, NY, USA) [23].

2.12 Western Blotting

Total proteins were extracted from cells and CRC tissues using RIPA buffer (Solarbio, Beijing, China). The extracted proteins were quantified via BCA assay, separated on 8–12% sodium dodecyl sulphate–polyacrylamide gels and transferred to polyvinylidene difluoride membranes. The membranes were initially incubated with anti-H2BC18 (1:1000, Boiss, Beijing, China) and anti-GAPDH (1:5000, Bioworld, Nanjing, China) primary antibodies and subsequently incubated with horseradish peroxidase (HRP)-conjugated anti-rabbit IgG antibody (secondary antibody, 1:5000, Bioworld, Nanjing, China). Finally, protein bands were visualised using an ECL reagent (Bioworld, Nanjing, China).

2.13 Immunohistochemical Analysis

The expression of H2BC18 in clinical tissues was assessed via immunohistochemical (IHC) analysis using anti-H2BC18 antibody (1:500, Boiss, Beijing, China), Paraffin-embedded tissue blocks were cut into 4-µm-thick sections, dewaxed, rehydrated using xylene I/II/III and anhydrous ethanol I/II/III (absolute ethyl alcohol) for 15 minutes each and washed with PBS two times for 5 minutes each. For antigen retrieval, tissue slides were placed in a sectioning rack and slowly immersed into an antigen repair solution. The solution was boiled on high for 5 min and on low for 20 min. Subsequently, the sections were washed with PBS two times for 10 minutes each, blocked with 3% bovine serum albumin (BSA) for 30 minutes at room temperature and incubated with primary antibodies overnight at 4 °C in a humidified incubator. The following day, the sections were washed with PBS (3 × 5 minutes) and incubated with HRP-conjugated anti-rabbit IgG antibody for 30 minutes at room temperature. Thereafter, the sections were washed with PBS (3 × 5 minutes) and stained with diaminobenzidine (DAB). Finally, the sections were observed under a white light microscope, and integrated OD (IOD) was calculated using the ImageJ software [23]. Data was expressed as the average OD (AOD), which was calculated as follows: IOD/area.

2.14 Statistical Analysis

The R (version 4.2.0) software (New York, NY, USA) was used for statistical analysis and visualisation of results. Student's *t*-test was used to compare normally distributed quantitative data and Wilcoxon test was used to compare non-normally distributed quantitative data between groups. Statistical significance was denoted as follows: *, $p < 0.05$; **, $p < 0.01$; ***, $p < 0.001$.

3. Results

3.1 Identification and Classification of Differentially Expressed NRGs in CRC

The gene expression data of 328 tissue samples, including 40 adjacent normal tissues and 288 CRC tissues, were extracted from TCGA database. A total of 1831 DEGs were identified between CRC and adjacent normal tissues (Fig. 1A); of which, 945 genes were upregulated and 886 genes were downregulated (Fig. 1B). These DEGs were intersected with 160 NRGs obtained from the GeneCards database using a Venn diagram, and 18 differentially expressed NRGs associated with CRC were eventually obtained (Fig. 1C). Subsequently, a consensus clustering algorithm was used to classify patients with CRC based on the expression of the 18 NRGs. With the optimal k value of 2, the patients were divided into cluster A and cluster B (Fig. 1D). Clinical characteristics (Fig. 1E) and NRG function were compared between the two clusters using Kaplan-Meier (K-M) analysis, immune infiltration analysis and GSVA. K-M curves showed that patients in cluster B had shorter OS than patients in cluster A (Fig. 1F). GSVA showed that cluster A was enriched in pathways related to inhibition of tumour development, including type I interferon signalling pathway and activation of mitochondrial autophagy, whereas cluster B was significantly enriched in tumour-promoting pathways such as DNA replication and chromatin aggregation (Fig. 1G). The infiltration levels of 22 types of immune cells differed significantly between the two clusters, with the infiltration levels of activated CD4 T cells and type 2 T helper cells (Th2) being higher in cluster A than in cluster B (Fig. 1H). These results suggested that the two clusters had different TME-associated properties and NRGs prolonged the OS of patients in cluster A by promoting anti-tumour immunity.

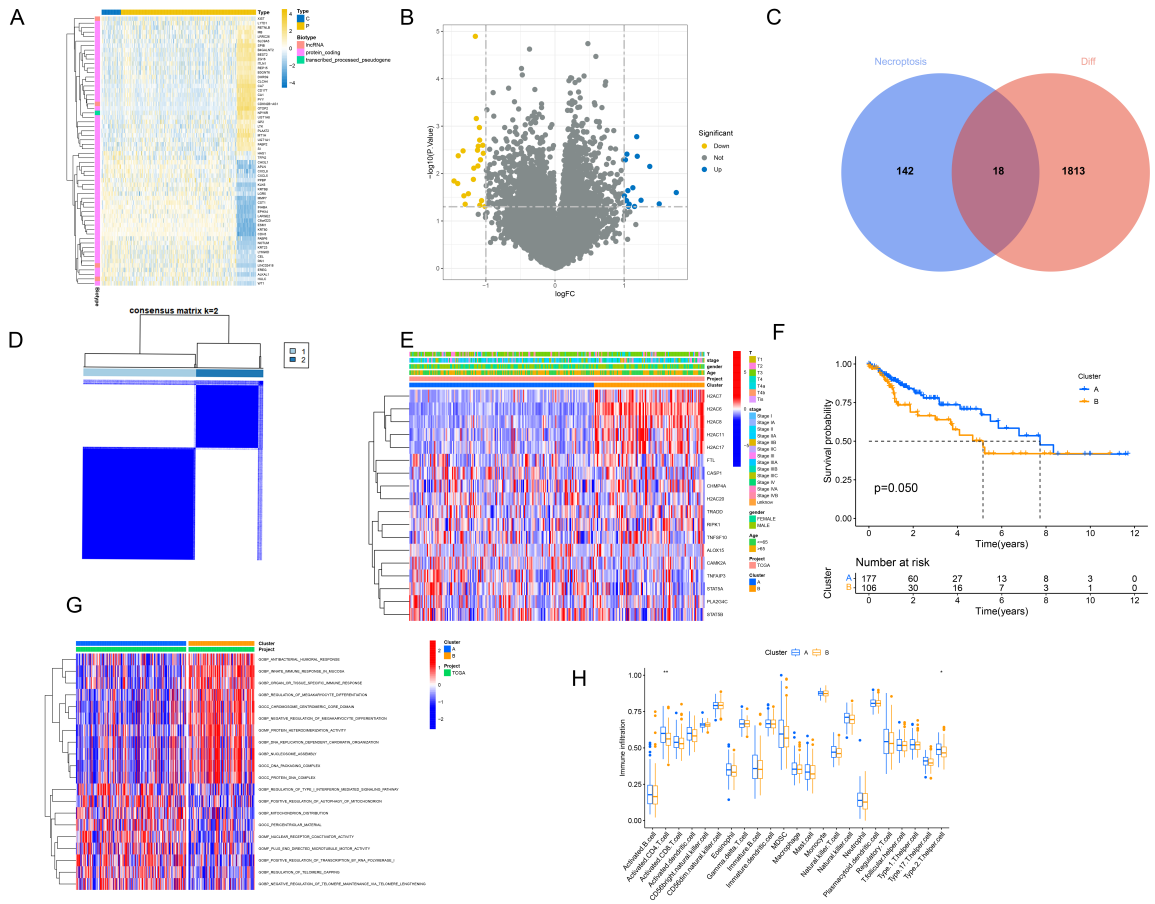

Fig. 1. Screening and categorisation of overall survival (OS)-related necroptosis-related genes (NRGs) in colorectal cancer (CRC). (A) Heatmap showing the top 60 differentially expressed genes (DEGs) (n = 1813) between CRC and adjacent normal tissue samples. (B) Volcano plot showing up-regulated (n = 945) and down-regulated genes (n = 886). (C) Venn diagram demonstrating the intersection between DEGs and necroptosis-related genes (n = 160). (D) Consensus matrix heatmap defining two clusters and associated regions. (E) Relationship of clusters A and B with clinicopathologic features and NRGs. (F) Kaplan-Meier curves (log-rank test, $p < 0.001$) of OS for clusters A and B. (G) GSVA of NRGs in clusters A and B. (H) Differences in the infiltration levels of 22 types of immune cells between the two clusters. Asterisks indicate *p*-values (*, $p < 0.05$; **, $p < 0.01$). GSVA, Gene Set Variation Analysis.

3.2 Construction and Evaluation of a Prognostic Model

Although the two molecular subtypes of necroptosis were found to have different prognostic and immune infiltration patterns, these findings are only applicable to patient populations and are not accurate for assessing the impact of NRGs on the prognosis of CRC. Therefore, we established a prognostic model based on the differentially expressed NRGs between clusters A and B for diagnosing CRC and guiding treatment. Briefly, we randomly divided patients with CRC into training (n = 287) and test (n = 41) sets and identified four NRGs significantly associated with CRC prognosis, namely, *CABPB1-IT1*, *H2BC18*, *HSPA1L* and *MIR503HG*, via LASSO regression analysis. The NRG-Score was calculated based on these four NRGs as follows: *GABPB1-IT1* expression level × 0.00260 + *H2BC18* expression level × 0.01596 + *HSPA1L* expression level × 0.02800 + *MIR503HG* expression level × 0.01304 (Fig. 2A,B). Based on the median NRG-Score, patients with CRC were divided into low-risk (n = 134) and high-risk (n = 149) groups. NRGs such as *CAMK2A*, *CASP1*, *CHMP4A*, *FTL*, *H2AC20*, *H2AC6*, *H2AC8*, *PLA2G4C*, *RIPK1*, *STAT5A/B* and *TRADD* were differentially expressed between the two groups (Fig. 2C). K-M curves showed that the prediction of prognosis was better in the low-risk group than in the high-risk group (Fig. 2D). Similar results were observed in the test set and the total-sample dataset (Fig. 2E,F). Subsequently, ROC curves were plotted to assess the predictive ability of the model. The results showed that the area under the curve (AUC) values for predicting OS at 1, 3 and 5 years were 0.641, 0.742 and 0.751, respectively, indicating that the model had excellent predictive ability, especially for 3- and 5-year survival (Fig. 2G–I). To assess the clinical applicability of the NRG-Score, we integrated NRG-Scores and

clinical characteristics such as age, sex and ISS stage to establish a nomogram to predict OS at 1, 3 and 5 years (Fig. 3A). The calibration curve showed that the predicted OS rates were highly consistent with the actual OS rates, indicating that the nomogram had superior predictive ability (Fig. 3B).

3.3 Immune Characterisation of Prognostic NRGs in the CRC Microenvironment

Studies have shown that necroptosis can promote cell death by enhancing tumour immunogenicity and that activation of the necroptotic factor RIPK1/RIPK3 can lead to upregulation of inflammatory chemokines in the TME, promoting immune cell activation [24–26]. Therefore, we investigated the association between the four NRGs and immune cell infiltration using the CIBERSORT algorithm. The four NRGs showed a significant correlation with most immune cells (Fig. 4A). In particular, a negative correlation was observed between the expression of NRGs and the infiltration levels of activated NK cells and $CD4^+$ memory T cells (Fig. 4B,C). These results suggested that the NRG-Score was markedly associated with the presence of TILs in the microenvironment of CRC and high-risk patients were susceptible to the immunosuppressive effects caused by the reduced abundance of activated NK and CD4 memory T cells in the TME. Furthermore, the expression of most immune checkpoint genes, including *CD274*, *CD70*, *HHLA2* and T*NFSF9*, was significantly higher in the low-risk group, and that of the leukocyte-associated immunoglobulin-producing gene *LAIR1* was significantly higher in the high-risk group (Fig. 4D). These results suggest that low-risk patients may respond better to LAIR1-targeted therapies, whereas high-risk patients may respond better to CD274- and CD70-targeted therapies.

3.4 Drug Sensitivity Analysis for NRGs Risk-prognostic Model

To examine the ability of NRG-Scores to guide the clinical treatment of CRC, we assessed the sensitivity of patients in the high- and low-risk groups to potential targeted drugs. The results showed that patients in the low-risk group responded better to LCK inhibitors (Fig. 5A), third-generation AKT inhibitors (Fig. 5B), JNK inhibitors (Fig. 5C) and the third-generation ABL inhibitor ponatinib (Fig. 5D), whereas patients in the high-risk group responded better to oral PARP inhibitors (Fig. 5E). Altogether, these findings suggest that the abovementioned drugs have potential therapeutic value in the treatment of CRC.

3.5 Expression Patterns of NRGs in CRC at the Single-cell Level

To assess the expression of prognosis-associated NRGs in the TME of CRC at the single-cell level, we extracted scRNA-sequencing data from the GSE4158911 and GSE4158912 datasets. After quality control and filtering, cells were classified as mast cells, fibroblasts, endothelial cells, epithelial cells and myeloid cells through dimensionality reduction (Fig. 6A,B). *HSPA1L* was highly expressed in fibroblasts and endothelial cells, whereas *MIR503HG* was highly expressed in epithelial cells. Given that CRC is a malignant tumour originating from epithelial cells, upregulated NRGs in epithelial cells may promote the transformation of normal epithelial cells to malignant tumour cells, suggesting that NRGs play an important role in the development of CRC (Fig. 6C).

3.6 Expression of Prognosis-related NRGs in CRC Cell Lines

To verify the differential expression and molecular functions of NRGs in CRC, we assessed the mRNA expression of the four prognosis-related NRGs (*GABPB1-IT1*, *H2BC18*, *HSPA1L* and *MIR503HG)* in three CRC cell lines (HCT15, HCT116 and HT29) and a normal colorectal epithelial cell line (NCM460). The expression of *GABPB1-IT1* (Fig. 7A), *HSPA1L* (Fig. 7B) and *MIR503HG* (Fig. 7C) was significantly lower in HCT15 and HCT116 cells than in NCM460 cells but was significantly higher in HT29 cells than in NCM460 cells. Only the expression of *H2BC18* was significantly higher in all three CRC cell lines than in the normal control cell line (Fig. 7D). Consistently, western blotting showed that the protein expression of H2BC18 was significantly elevated in the three CRC cell lines (Fig. 7E). Clinical tissue samples, including 3 CRC and colorectal inflammation tissues, were collected to verify these results. Immunohistochemical (IHC) analysis showed that the protein expression of H2BC18 was higher in CRC tissues than in colorectal inflammation tissues (Fig. 7F). In addition, IHC data from the Human Protein Atls (HPA) database validated the differential expression of H2BC18 protein between CRC and colorectal inflammation tissues (Fig. 7G). Altogether, these results suggest that *H2BC18* plays an important role as a prognosis-associated gene in CRC. Therefore, in subsequent experiments, we examined the biological function of H2BC18 in CRC progression.

3.7 H2BC18 Promotes the Proliferative, Invasive and Migratory Abilities of CRC Cells

To assess the effects of *H2BC18* on the malignant progression of CRC, HCT15 cells were transiently transfected with an siRNA targeting *H2BC18*. The proliferative, invasive and migratory abilities of CRC cells were examined after the successful knockdown of *H2BC18* (Fig. 8A). CCK-8 assay showed that knockdown of *H2BC18* inhibited the proliferation of HCT15 cells (Fig. 8B). In addition, wound healing and transwell invasion assays showed that knockdown of *H2BC18* significantly inhibited the migratory and invasive abilities of HCT15 cells (Fig. 8B–D). Altogether, these results suggest that *H2BC18* plays an important role in regulating the malignant progression of CRC.

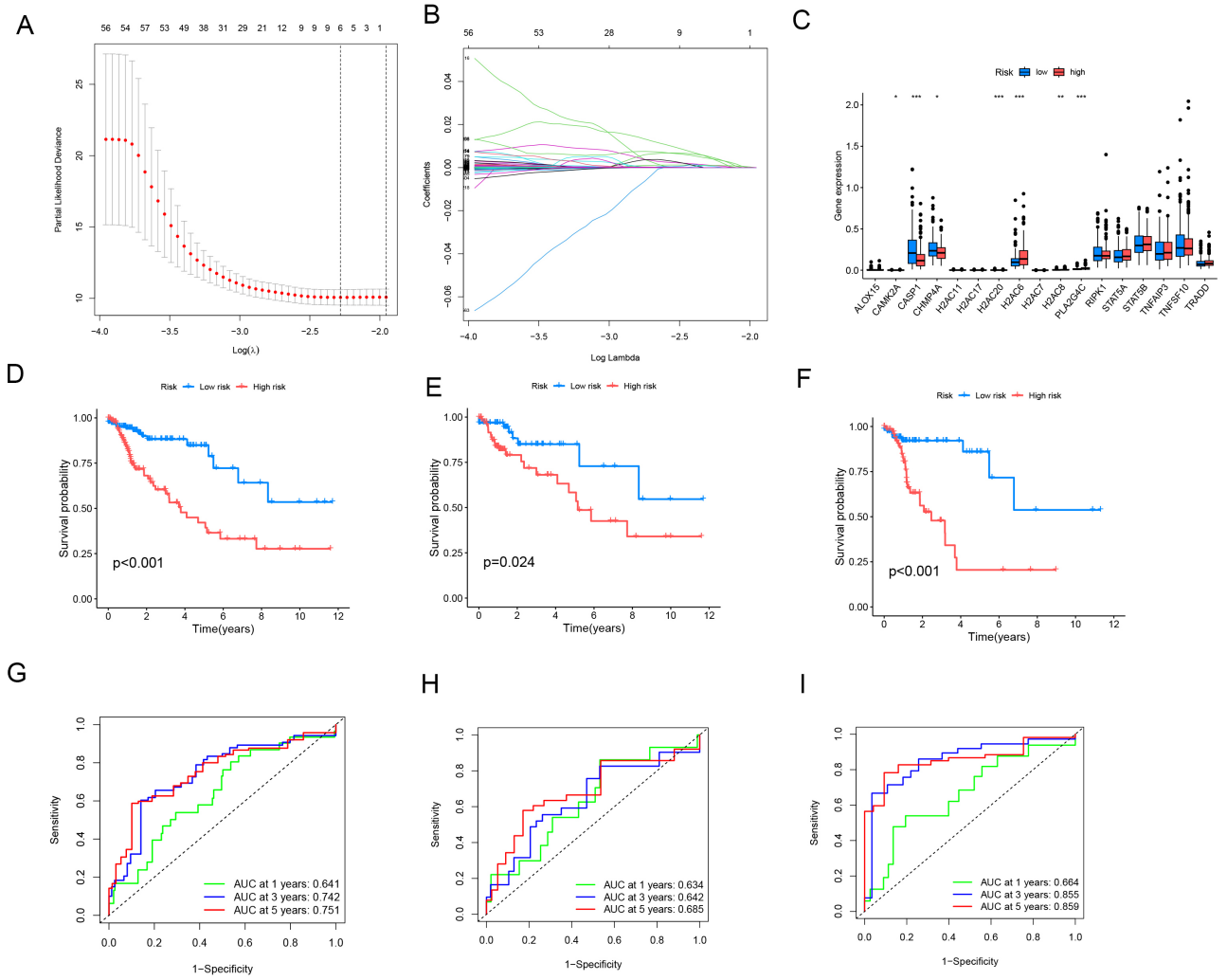

Fig. 2. Construction and evaluation of a prognostic model. (A) 1000-fold cross-validation for the selection of LASSO regression variables. (B) LASSO regression coefficients of necroptosis-related genes. Each curve corresponds to a gene involved in necroptosis. (C) Expression of 18 OS-associated NRGs in the high- and low-risk groups. (D) Kaplan-Meier (K-M) survival curves for the low- and high-risk groups in the training set. (E) K-M survival curves for the low- and high-risk groups in the test set. (F) K-M survival curves for the low- and high-risk groups in the total-sample dataset. (G) Receiver operating characteristic (ROC) curves for predicting 1-, 3- and 5-year OS in the training set. (H) Receiver operating characteristic (ROC) curves for predicting 1-, 3- and 5-year OS in the test set. (I) Receiver operating characteristic (ROC) curves for predicting 1-, 3- and 5-year OS in the total-sample dataset. (*, $p < 0.05$; **, $p < 0.01$; ***, $p < 0.001$). LASSO, least absolute shrinkage and selection operator.

4. Discussion

CRC is one of the three most prevalent malignant tumours worldwide [27], with the second-highest mortality rate [1]. Metastasis and the failure of early diagnosis leading that the 5-year survival rate of patients with CRC is <15% [28]. Necroptosis, a novel programmed cell death mechanism, has been associated with the development of intestinal diseases and reported to play a dual role in tumorigenesis. In this study, we investigated the effects of NRGs on the prognosis of CRC and characterised their specific expression patterns and molecular functions in CRC.

We analysed the relationship between NRGs and CRC. In the TCGA dataset, NRGs were found to be differentially expressed between CRC and normal adjacent tissues and correlated with the prognosis of CRC. Two molecular subtypes were classified based on the expression patterns of 18 NRGs. These subtypes showed significant differences in prognosis, immune cell infiltration and molecular functions of NRGs. In terms of prognosis, patients in cluster A had longer OS than those in cluster B. In terms of immune infiltration, the abundance of $CD4^+$ T cells and Th2 cells was higher in cluster A. Several previous studies have shown that high infiltration levels of $CD4^+$ T cells are associated with a favourable prognosis in tumours, such as lung cancer [29]. Th2 cells can directly block spontaneous breast cancer development by inducing terminal differen-

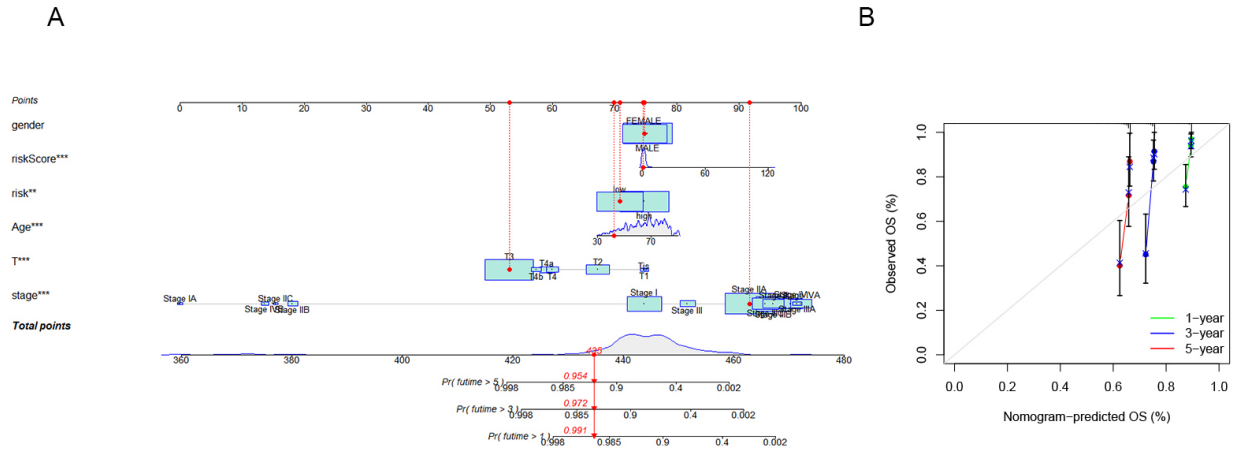

Fig. 3. Development and validation of the nomogram. (A) Nomogram integrating NRG-Scores and clinical characteristics such as age, sex, TNM and stage for predicting 1-, 3- and 5-year OS. (B) Calibration curve demonstrating the accuracy of the nomogram in predicting survival at 1, 3 and 5 years. The dashed line represents the performance of an ideal nomogram, whereas the solid green, blue and red lines indicate the performance of the established nomogram. **, $p < 0.01$; ***, $p < 0.001$. TNM, Tumor Node Metastasis.

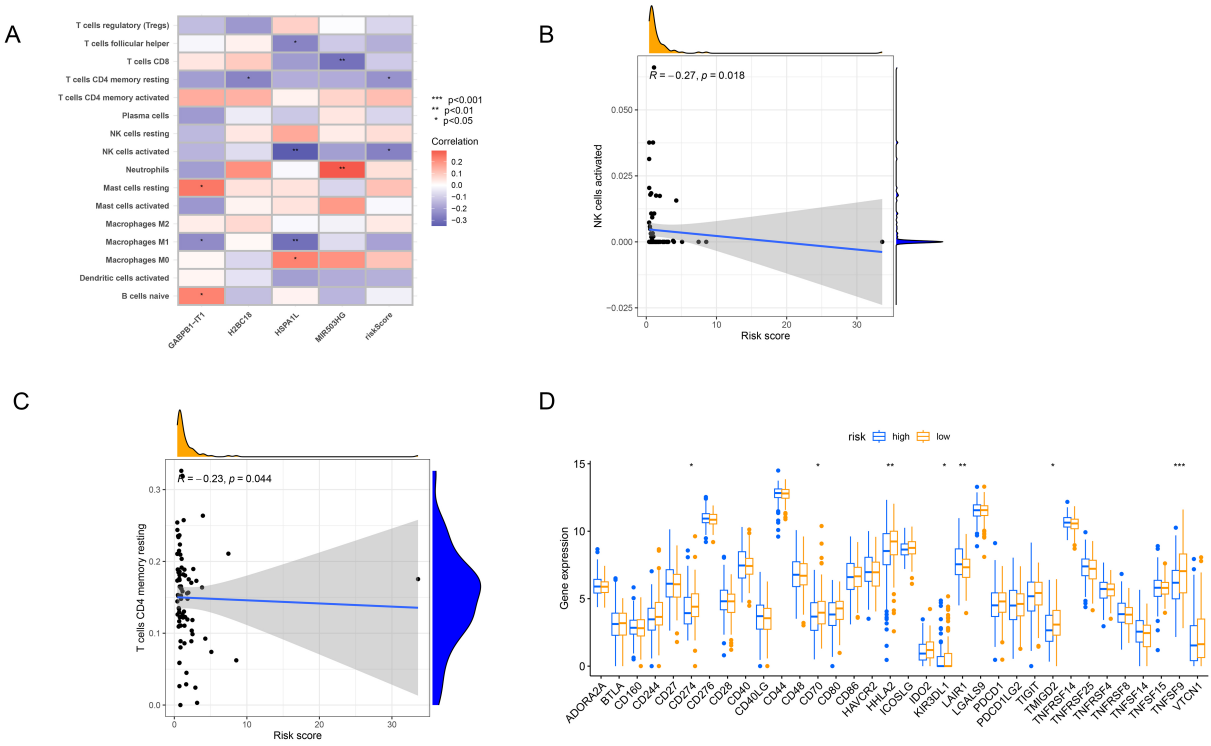

Fig. 4. Immune characterisation of prognostic NRGs in the CRC microenvironment. (A) Correlation between the expression of the four NRGs and the abundance of tumour-infiltrating immune cells. (B) Correlation between the abundance of activated Nature Killer (NK) cells and NRG-Scores. (C) Correlation between the abundance of $CD4^+$ memory T cells and NRG-Scores. (D) Histogram demonstrating differences in the expression of immune checkpoints between the high- and low-risk groups. Yellow and blue columns indicate the low- and high-risk groups, respectively (*, $p < 0.05$; **, $p < 0.01$; ***, $p < 0.001$).

tiation of cancer cells [30]. GSVA showed that cluster A was mainly enriched in pathways associated with the inhibition of tumour development, including the type I interferon signalling pathway and activation of mitochondrial autophagy [31,32]. On the contrary, cluster B was enriched in pathways associated with the promotion of tumour development, including DNA replication, chromatin aggregation and nucleosome assembly [33]. Taken together with the characteristics of immune infiltration of the two subtypes, these results validated that patients in cluster A had longer OS.

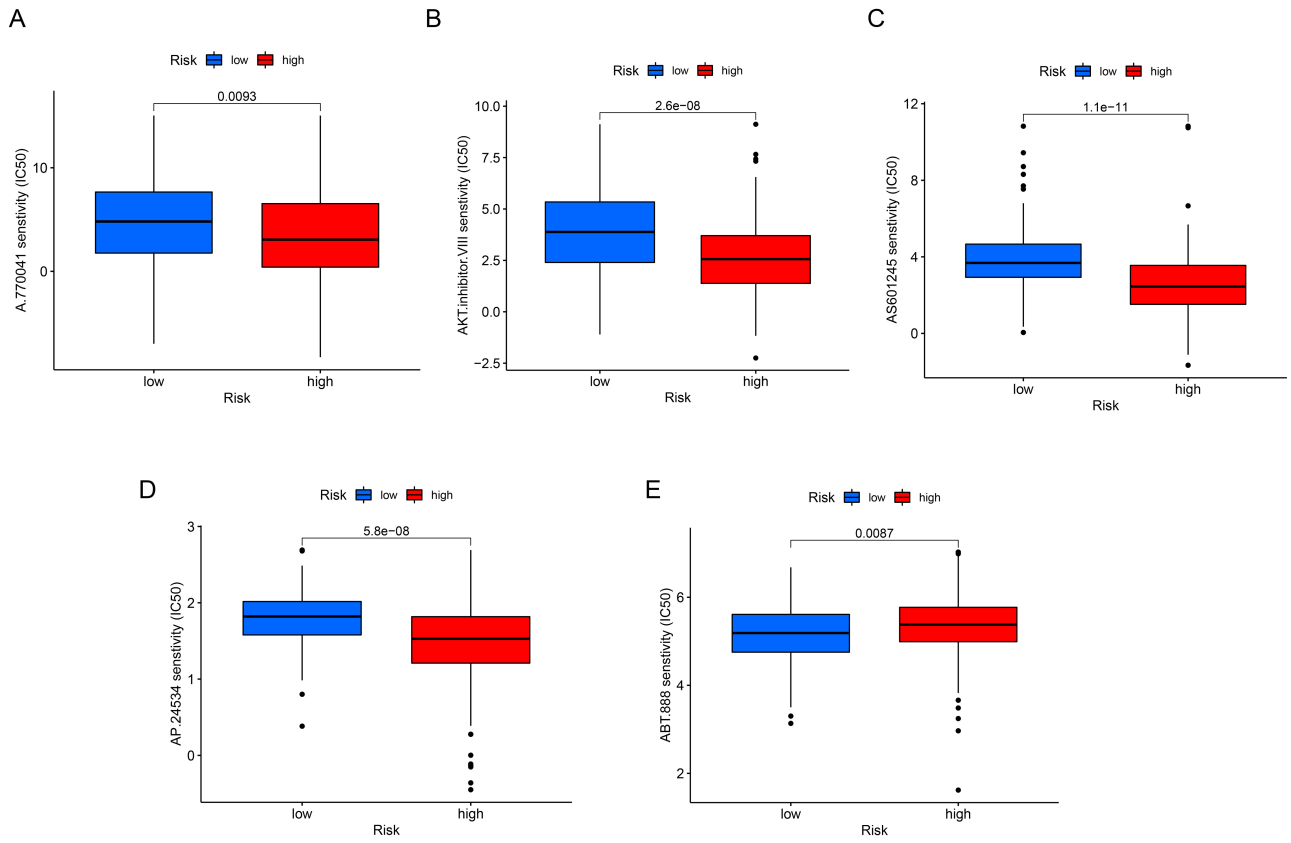

Fig. 5. Drug sensitivity analysis in the high- and low-risk groups. (A) Differences in the expression of LCK inhibitors between the high- and low-risk groups. (B) Differences in the expression of AKT inhibitors between the high- and low-risk groups. (C) Differences in the expression of JNK inhibitors between the high- and low-risk groups. (D) Differences in the expression of the third-generation ABL inhibitor ponatinib between the high- and low-risk groups. (E) Differences in the expression of PARP inhibitors between the high- and low-risk groups.

Furthermore, we developed a prognostic risk model (NRG-Score) based on four differentially expressed prognosis-associated NRGs, namely, *H2BC18*, *HSPA1L*, *MIR503HG* and *GABPB1-IT1*. Subsequently, a nomogram integrating the NRG-Score and clinicopathologic features was established to predict the OS of patients with CRC. The calibration curve demonstrated that the nomogram had superior predictive performance, especially for long-term survival. Unlike in other studies [34], in this study, patients with CRC were divided into training, test and total-sample validation sets, and the predictive accuracy and validity of the prognostic model were verified by evaluating the AUC values of each group. Altogether, the results suggested that the prognostic model had better predictive accuracy. The four NRGs included in the model have been shown to play important roles in cancer [35–42], suggesting that the NRG-Score developed in this study is closely related to the development and prognosis of CRC.

The TME is a complex ecosystem composed of many different cell populations, and its composition is closely related to the prognosis and treatment response of patients with CRC [43]. Many studies have reported that the OS and progression-free survival (PFS) of patients with CRC can be predicted based on the type, spatial location and infiltration levels of immune cells [44–46]. To examine the effects of the four prognostic NRGs on the immune microenvironment of CRC, patients were divided into high- and low-risk groups based on the median NRG-Score. The abundance of tumour-infiltrating immune cells in the TME, expression of immune checkpoint genes and sensitivity to targeted drugs were significantly different between the low- and high-risk groups.

The interaction between immune and cancer cells in the TME is important for tumour progression and drug resistance [47]. Therefore, we examined the association between the four NRGs and immune cell infiltration using the CIBERSORT algorithm. It was found that the expression of NRGs was significantly associated with the abundance of most immune cells. In particular, the expression of NRGs was negatively correlated with the abundance of NK cells and CD4+ memory T cells. NK cells perform multiple functions in the human body. Infiltration of NK cell indicates a better prognosis in gastric cancer and squamous cell carcinoma, suggesting that NK cells have anti-tumour

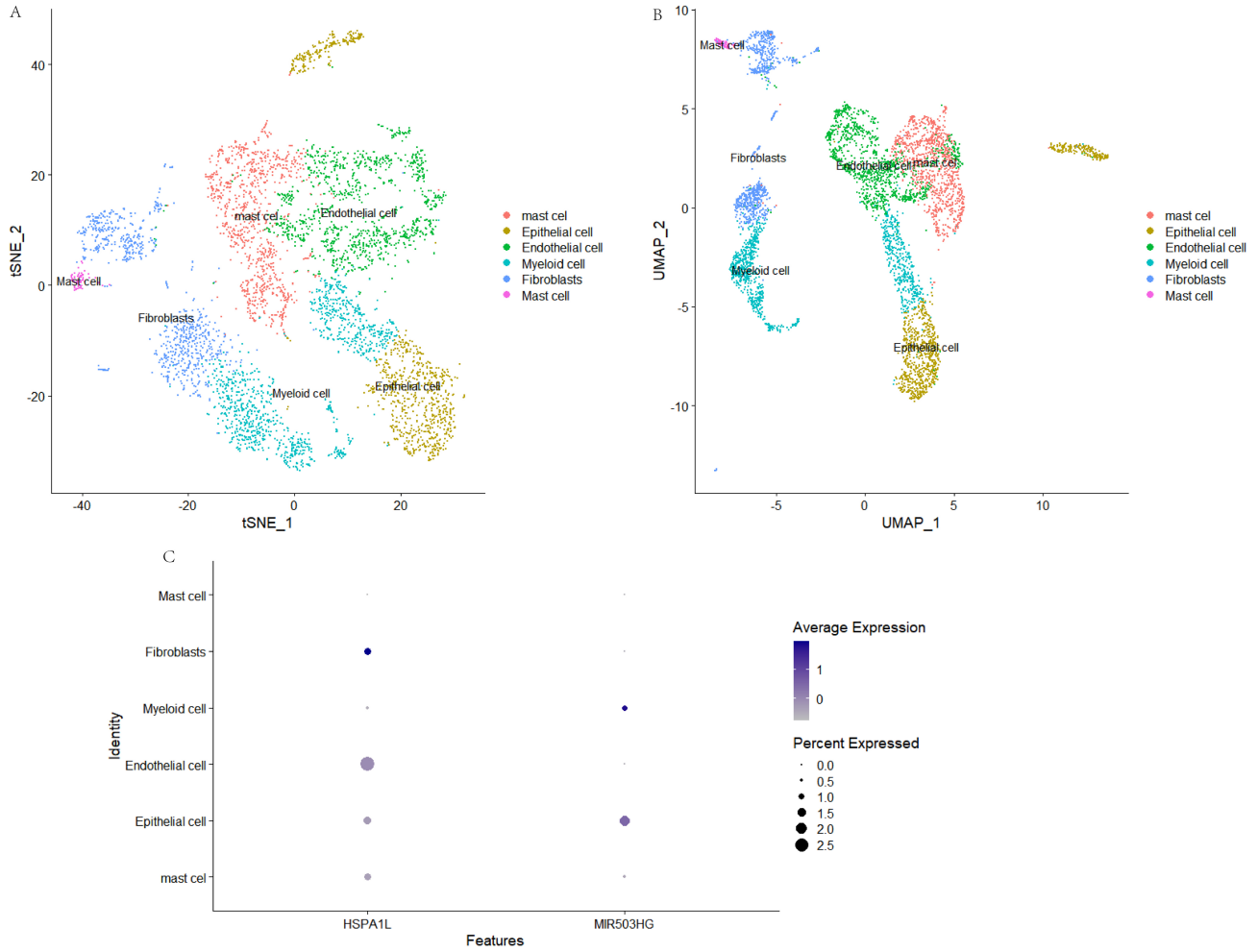

Fig. 6. Analysis of the expression of NRGs in cell clusters using scRNA-sequencing data. (A) Cell clusters annotated in the GSE4158911 dataset. (B) Cell clusters annotated in the GSE4158912 dataset. (C) Differential expression of two prognostically relevant NRGs in six cell clusters.

activity [48]. CD4 T cells can kill tumour cells directly through anti-specific [49,50] cytolytic mechanisms or indirectly by modulating the TME. These findings suggest that the low abundance of activated NK cells and CD4 memory T cells in the TME of patients in the high-risk group may lead to a worse prognosis. Single-cell analysis showed the significantly higher expression of *HSPA1L* and *MIR503HG* in epithelial cells, fibroblasts and endothelial cells, suggesting that these NRGs mediate the depletion of NK and CD4 memory T cells through epithelial cells and fibroblasts, thus contributing to the immunosuppressive microenvironment of CRC. In addition, most immune checkpoint genes (*CD160*, *CD80*, *HHLA2* and *CD244*) were significantly lower in the high-risk group, suggesting that patients in this group may benefit more from immune checkpoint inhibitor therapy targeting these genes. In order to screen for potential targeted drugs for the treatment of CRC, Drug sensitivity analysis was performed to identify potential targeted drugs for the treatment of CRC. The results showed that patients in the low-risk group were more sensitive to LCK inhibitors, third-generation AKT inhibitors, JNK inhibitors and the third-generation ABL inhibitor ponatinib, whereas those in the high-risk group were more sensitive to oral PARP inhibitors, which are effective in inhibiting DNA repair in CRC cells [51,52] and are currently used to improve radiosensitivity in clinical practice.

The expression of the four NRGs was evaluated in three CRC cell lines (HCT15, HCT116 and HT29). *HSPA1L*, *MIR503HG* and *GABPB1-IT1* were differently expressed in the three cell lines. In particular, the expression of the three NRGs was low in HCT15 and HCT116 cells but high in HT29 cells. This differential expression may be related to the dual role of necroptosis in CRC and the heterogeneity among different CRC subtypes. On the contrary, the expression of *H2BC18* was significantly elevated in all three cell lines, suggesting that *H2BC18* plays an important role in regulating the development of CRC. The protein expression of H2BC18 in CRC cells and tissues was analysed via WB and IHC analysis and validated using IHC data from the HPA database. We found that the protein

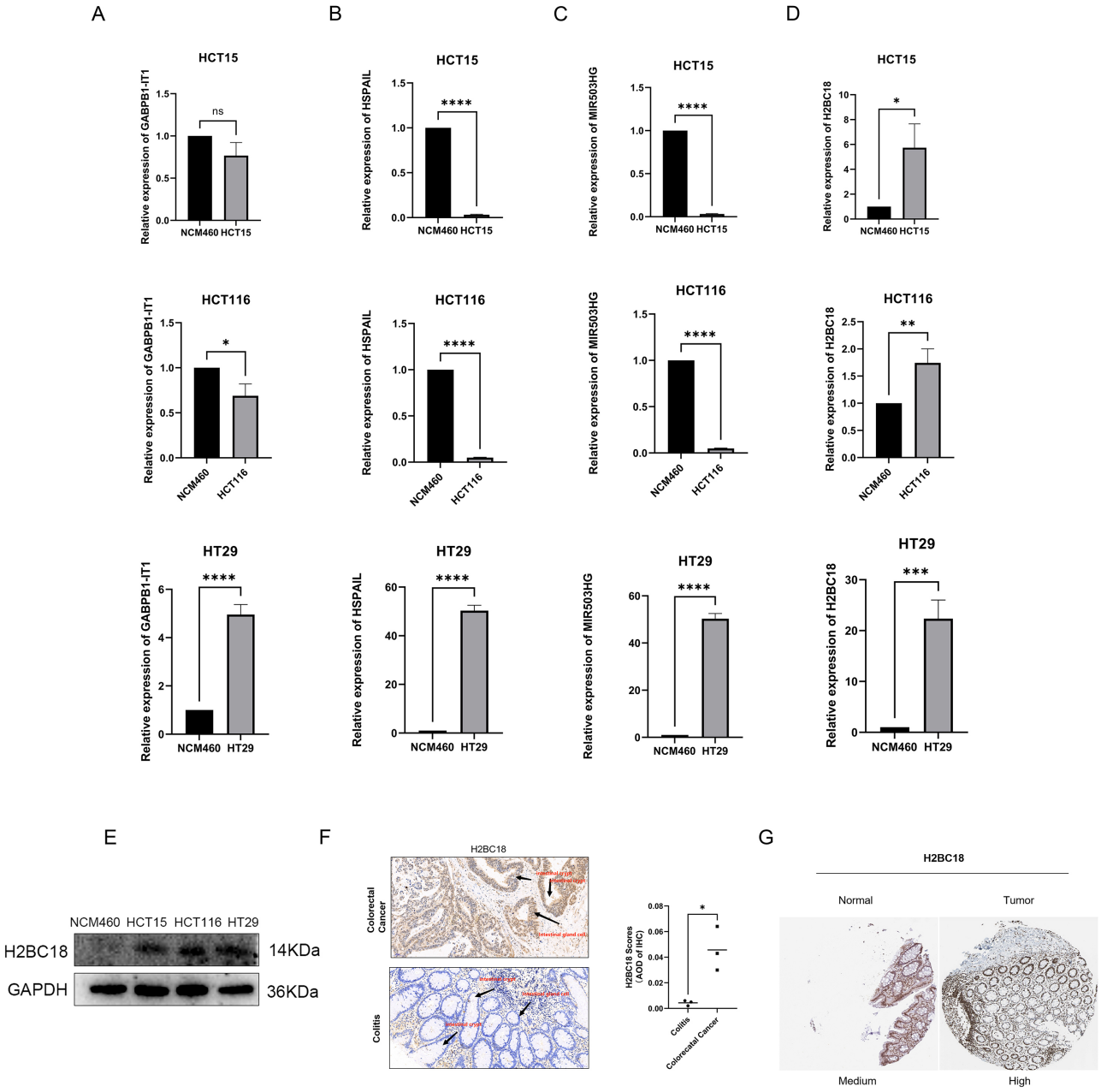

Fig. 7. Expression of prognosis-related NRGs in colorectal cancer (CRC) cell lines. (A) Expression of *GABPB1-IT1* in CRC cells versus NCM460 cells. (B) Expression of *HSPA1L* in CRC cells versus NCM460 cells. (C) Expression of *MIR503HG* in CRC cells versus NCM460 cells. (D) Expression of *H2BC18* in CRC cells versus NCM460 cells (*, $p < 0.05$; **, $p < 0.01$; ****, $p < 0.0001$; ns means the difference between the two groups was not statistically significant. Each experiment was repeated three times). (E) Western blotting was performed to evaluate the protein expression of H2BC18 in three CRC cell lines. (F) Comparison of H2BC18 expression between CRC tissues and colorectal inflammation tissues via immunohistochemical (IHC) analysis. (G) Comparison of H2BC18 expression between CRC tissues and adjacent normal tissues using IHC data from the HPA database. Tumor image available from: https://images.proteinatlas.org/7814/18508_A_8_3.jpg and Normal image available from: https://images.proteinatlas.org/48671/113841_A_7_3.jpg.

expression of H2BC18 was higher in CRC cells than in normal colon cells as well as in CRC tissues than in adjacent normal tissues. Finally, we preliminarily examined the biological functions of *H2BC18* in the malignant progression of CRC. The invasive, migratory and proliferative abilities of HCT15 cells were significantly weaker in the H2BC18-knockdown group than in the control group, indicating that the NRG *H2BC18* plays a more important regulatory role in the development of CRC.

In conclusion, we developed and validated the NRG-Score prognostic model and examined the potential biological effects of the NRGs included in this model on the

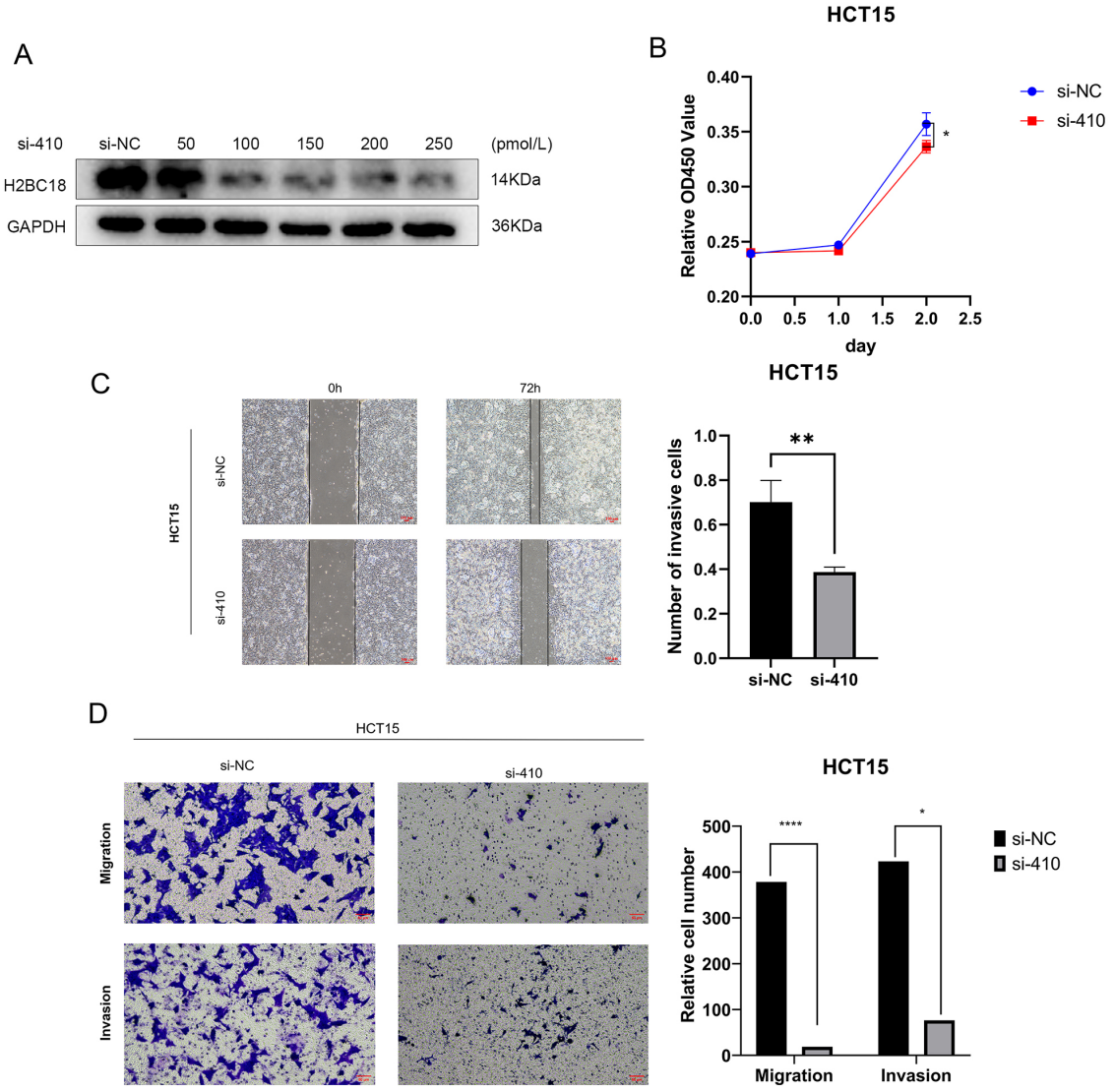

Fig. 8. H2BC18 regulates the proliferative, invasive and migratory abilities of CRC cells. (A) Western blotting was performed to detect the efficiency of H2BC18 knockdown in HCT15 cells. (B) CCK-8 assay was performed to examine the proliferative ability (OD450) of CRC cells after *H2BC18* knockdown. (C) Wound healing assay was performed to examine the migratory ability of CRC cells after *H2BC18* knockdown. (D) Transwell assay was performed to examine the invasive and migratory abilities of CRC cells after *H2BC18* knockdown (*, $p < 0.05$; **, $p < 0.01$; ****, $p < 0.0001$).

immune microenvironment of CRC. The model accurately predicted the OS of patients with CRC and their sensitivity to common chemotherapeutic agents and improved individual prognostic monitoring. Therefore, the model may guide the development of novel NRG-targeted therapies for CRC.

5. Conclusion

In this study, we performed an in-depth analysis of the expression of NRGs in CRC and identified and characterised two molecular subtypes based on the expression patterns of NRGs. In addition, we established the NRG-Score and found that patients with CRC with low NRG-Scores had a better prognosis. On evaluating the available biomarkers that could be used for immunotherapy, we found that patients with high NRG-Scores might benefit more from immunotherapy. These findings improve our understanding of TME and immune cell infiltration in CRC and may guide the development of more effective immunotherapies and targeted therapies. However, this study has some limitations that should be acknowledged. First, elucidating the precise role of each NRG in CRC requires multi-omic data and an in-depth understanding of molecular mechanisms. Second, the four core NRGs warrant further validation in preclinical studies. Therefore, large-sample, prospective cohort studies as well as *in vivo* and *in vitro* experimental studies should be conducted to validate the predictive accuracy of the NRG-Score.

Availability of Data and Materials

The datasets generated during the current study are available from the supplementary information or the corresponding author upon reasonable request. The datasets supporting the conclusions of this article are available in the The Cancer Genome Atlas (TCGA) database (https://www.cancer.gov/ccg/research/genome-sequencing/tcga), TCGA-CRC, GSE4158911, GSE4158912.

Author Contributions

QL, ML, YH and LL conceived and coordinated the study. YH and LL wrote and revised the paper. YH, LL, ZK, HLuo, XL, SZ and QZ analysed the experiments. QL, ML and HLiu offered technical or material support for the experiments, critical reading, and text revisions. All authors contributed to editorial changes in the manuscript. All authors reviewed the results and approved the final version of the manuscript. All authors have participated sufficiently in the work and agreed to be accountable for all aspects of the work.

Ethics Approval and Consent to Participate

Not applicable.

Acknowledgment

We thank Bullet Edits Limited for the linguistic editing and proofreading of the manuscript.

Funding

The present study was supported by the National Natural Science Foundation of China (81960476, 81460365, 81760039, 82173378), Guizhou Provincial Science and Technology Projects ([2019]1270), Guizhou Provincial Health and Health Commission Fund (gzwkj2021-160), and Guizhou Medical University Science and Technology Projects (21NSFCP12).

Conflict of Interest

The authors declare no conflict of interest.

References

[1] Sung H, Ferlay J, Siegel RL, Laversanne M, Soerjomataram I, Jemal A, *et al*. Global Cancer Statistics 2020: GLOBOCAN Estimates of Incidence and Mortality Worldwide for 36 Cancers in 185 Countries. CA: a Cancer Journal for Clinicians. 2021; 71: 209–249.

[2] Bénard F, Barkun AN, Martel M, von Renteln D. Systematic review of colorectal cancer screening guidelines for average-risk adults: Summarizing the current global recommendations. World Journal of Gastroenterology. 2018; 24: 124–138.

[3] Morgan E, Arnold M, Gini A, Lorenzoni V, Cabasag CJ, Laversanne M, *et al*. Global burden of colorectal cancer in 2020 and 2040: incidence and mortality estimates from GLOBOCAN. Gut. 2023; 72: 338–344.

[4] Degterev A, Huang Z, Boyce M, Li Y, Jagtap P, Mizushima N, *et al*. Chemical inhibitor of nonapoptotic cell death with therapeutic potential for ischemic brain injury. Nature Chemical Biology. 2005; 1: 112–119.

[5] Gong Y, Fan Z, Luo G, Yang C, Huang Q, Fan K, *et al*. The role of necroptosis in cancer biology and therapy. Molecular Cancer. 2019; 18: 100.

[6] Kearney CJ, Cullen SP, Clancy D, Martin SJ. RIPK1 can function as an inhibitor rather than an initiator of RIPK3-dependent necroptosis. The FEBS Journal. 2014; 281: 4921–4934.

[7] Zhou P, Zhang S, Wang M, Zhou J. The Induction Mechanism of Ferroptosis, Necroptosis, and Pyroptosis in Inflammatory Bowel Disease, Colorectal Cancer, and Intestinal Injury. Biomolecules. 2023; 13: 820.

[8] Han Q, Ma Y, Wang H, Dai Y, Chen C, Liu Y, *et al*. Resibufogenin suppresses colorectal cancer growth and metastasis through RIP3-mediated necroptosis. Journal of Translational Medicine. 2018; 16: 201.

[9] Zhang Z, Ju F, Chen F, Wu H, Chen J, Zhong J, *et al*. GDC-0326 Enhances the Effects of 5-Fu in Colorectal Cancer Cells by Inducing Necroptotic Death. OncoTargets and Therapy. 2021; 14: 2519–2530.

[10] Wang Y, Zhao M, He S, Luo Y, Zhao Y, Cheng J, *et al*. Necroptosis regulates tumor repopulation after radiotherapy via RIP1/RIP3/MLKL/JNK/IL8 pathway. Journal of Experimental & Clinical Cancer Research: CR. 2019; 38: 461.

[11] Gautier L, Cope L, Bolstad BM, Irizarry RA. affy–analysis of Affymetrix GeneChip data at the probe level. Bioinformatics (Oxford, England). 2004; 20: 307–315.

[12] Leek JT, Johnson WE, Parker HS, Jaffe AE, Storey JD. The sva package for removing batch effects and other unwanted variation in high-throughput experiments. Bioinformatics (Oxford, England). 2012; 28: 882–883.

[13] Ritchie ME, Phipson B, Wu D, Hu Y, Law CW, Shi W, *et al*. limma powers differential expression analyses for RNA-sequencing and microarray studies. Nucleic Acids Research. 2015; 43: e47.

[14] Wilkerson MD, Hayes DN. ConsensusClusterPlus: a class discovery tool with confidence assessments and item tracking. Bioinformatics (Oxford, England). 2010; 26: 1572–1573.

[15] Hänzelmann S, Castelo R, Guinney J. GSVA: gene set variation analysis for microarray and RNA-seq data. BMC Bioinformatics. 2013; 14: 7.

[16] Newman AM, Liu CL, Green MR, Gentles AJ, Feng W, Xu Y, *et al*. Robust enumeration of cell subsets from tissue expression profiles. Nature Methods. 2015; 12: 453–457.

[17] Fontanarosa JB, Dai Y. Using LASSO regression to detect predictive aggregate effects in genetic studies. BMC Proceedings. 2011; 5: S69.

[18] Vrieze SI. Model selection and psychological theory: a discussion of the differences between the Akaike information criterion (AIC) and the Bayesian information criterion (BIC). Psychological Methods. 2012; 17: 228–243.

[19] Zhang Z, Kattan MW. Drawing Nomograms with R: applications to categorical outcome and survival data. Annals of Translational Medicine. 2017; 5: 211.

[20] Alba AC, Agoritsas T, Walsh M, Hanna S, Iorio A, Devereaux PJ, *et al*. Discrimination and Calibration of Clinical Prediction Models: Users' Guides to the Medical Literature. JAMA. 2017; 318: 1377–1384.

[21] Geeleher P, Cox N, Huang RS. pRRophetic: an R package for prediction of clinical chemotherapeutic response from tumor gene expression levels. PloS One. 2014; 9: e107468.

[22] Livak KJ, Schmittgen TD. Analysis of relative gene expression data using real-time quantitative PCR and the 2(-Delta Delta C(T)) Method. Methods (San Diego, Calif.). 2001; 25: 402–408.

[23] Schneider CA, Rasband WS, Eliceiri KW. NIH Image to ImageJ: 25 years of image analysis. Nature Methods. 2012; 9: 671–675.

[24] Yatim N, Jusforgues-Saklani H, Orozco S, Schulz O, Barreira da Silva R, Reis e Sousa C, *et al*. RIPK1 and NF-κB signaling in dying cells determines cross-priming of $CD8^+$ T cells. Science (New York, N.Y.). 2015; 350: 328–334.
[25] Harlin H, Meng Y, Peterson AC, Zha Y, Tretiakova M, Slingluff C, *et al*. Chemokine expression in melanoma metastases associated with CD8+ T-cell recruitment. Cancer Research. 2009; 69: 3077–3085.
[26] Park HH, Kim HR, Park SY, Hwang SM, Hong SM, Park S, *et al*. RIPK3 activation induces TRIM28 derepression in cancer cells and enhances the anti-tumor microenvironment. Molecular Cancer. 2021; 20: 107.
[27] Jemal A, Siegel R, Ward E, Murray T, Xu J, Thun MJ. Cancer statistics, 2007. CA: a Cancer Journal for Clinicians. 2007; 57: 43–66.
[28] Quan J, Ma C, Sun P, Wang S, Zhuang M, Liu Z, *et al*. Brain metastasis from colorectal cancer: clinical characteristics, timing, survival and prognostic factors. Scandinavian Journal of Gastroenterology. 2019; 54: 1370–1375.
[29] Eberst G, Vernerey D, Laheurte C, Meurisse A, Kaulek V, Cuche L, *et al*. Prognostic value of CD4+ T lymphopenia in non-small cell lung Cancer. BMC Cancer. 2022; 22: 529.
[30] Rochman Y, Dienger-Stambaugh K, Richgels PK, Lewkowich IP, Kartashov AV, Barski A, *et al*. TSLP signaling in $CD4^+$ T cells programs a pathogenic T helper 2 cell state. Science Signaling. 2018; 11: eaam8858.
[31] Shou P, Chen Q, Jiang J, Xu C, Zhang J, Zheng C, *et al*. Type I interferons exert anti-tumor effect via reversing immunosuppression mediated by mesenchymal stromal cells. Oncogene. 2016; 35: 5953–5962.
[32] Vara-Perez M, Felipe-Abrio B, Agostinis P. Mitophagy in Cancer: A Tale of Adaptation. Cells. 2019; 8: 493.
[33] Ding Y, Li N, Dong B, Guo W, Wei H, Chen Q, *et al*. Chromatin remodeling ATPase BRG1 and PTEN are synthetic lethal in prostate cancer. The Journal of Clinical Investigation. 2019; 129: 759–773.
[34] Yuan Y, Chen J, Wang J, Xu M, Zhang Y, Sun P, *et al*. Development and Clinical Validation of a Novel 4-Gene Prognostic Signature Predicting Survival in Colorectal Cancer. Frontiers in Oncology. 2020; 10: 595.
[35] Choi SI, Lee JH, Kim RK, Jung U, Kahm YJ, Cho EW, *et al*. HSPA1L Enhances Cancer Stem Cell-Like Properties by Activating IGF1Rβ and Regulating β-Catenin Transcription. International Journal of Molecular Sciences. 2020; 21: 6957.
[36] Najafi M, Mortezaee K, Majidpoor J. Cancer stem cell (CSC) resistance drivers. Life Sciences. 2019; 234: 116781.
[37] Lee JH, Han YS, Yoon YM, Yun CW, Yun SP, Kim SM, *et al*. Role of HSPA1L as a cellular prion protein stabilizer in tumor progression via HIF-1α/GP78 axis. Oncogene. 2017; 36: 6555–6567.
[38] Tian J, Yang L, Wang Z, Yan H. MIR503HG impeded ovarian cancer progression by interacting with SPI1 and preventing TMEFF1 transcription. Aging. 2022; 14: 5390–5405.
[39] Chuo D, Liu F, Chen Y, Yin M. LncRNA MIR503HG is downregulated in Han Chinese with colorectal cancer and inhibits cell migration and invasion mediated by TGF-β2. Gene. 2019; 713: 143960.
[40] Gong TY, Chen HY, Liu ZH. MIR503HG promotes esophageal squamous cell carcinoma cell proliferation, invasion and migration via hsa-miR-503 pathway. Zhonghua Zhong Liu Za Zhi [Chinese Journal of Oncology]. 2022; 44: 1160–1167. (In Chinese)
[41] Tan C, Du H, Wang Y, Zhao J, Cheng X, Lan H. LncRNA GABPB1-IT1 inhibits the tumorigenesis of renal cancer via the miR-21/PTEN axis. Journal of Biochemical and Molecular Toxicology. 2023; 37: e23288.
[42] Jia J, Han Z, Wang X, Zheng X, Wang S, Cui Y. H2B gene family: A prognostic biomarker and correlates with immune infiltration in glioma. Frontiers in Oncology. 2022; 12: 966817.
[43] Wang W, Zhong Y, Zhuang Z, Xie J, Lu Y, Huang C, *et al*. Multiregion single-cell sequencing reveals the transcriptional landscape of the immune microenvironment of colorectal cancer. Clinical and Translational Medicine. 2021; 11: e253.
[44] Pagès F, Mlecnik B, Marliot F, Bindea G, Ou FS, Bifulco C, *et al*. International validation of the consensus Immunoscore for the classification of colon cancer: a prognostic and accuracy study. Lancet (London, England). 2018; 391: 2128–2139.
[45] de Vries NL, van Unen V, Ijsselsteijn ME, Abdelaal T, van der Breggen R, Farina Sarasqueta A, *et al*. High-dimensional cytometric analysis of colorectal cancer reveals novel mediators of antitumour immunity. Gut. 2020; 69: 691–703.
[46] Zhang L, Zhao Y, Dai Y, Cheng JN, Gong Z, Feng Y, *et al*. Immune Landscape of Colorectal Cancer Tumor Microenvironment from Different Primary Tumor Location. Frontiers in Immunology. 2018; 9: 1578.
[47] Jin MZ, Jin WL. The updated landscape of tumor microenvironment and drug repurposing. Signal Transduction and Targeted Therapy. 2020; 5: 166.
[48] Ishigami S, Natsugoe S, Tokuda K, Nakajo A, Che X, Iwashige H, *et al*. Prognostic value of intratumoral natural killer cells in gastric carcinoma. Cancer. 2000; 88: 577–583.
[49] Kruse B, Buzzai AC, Shridhar N, Braun AD, Gellert S, Knauth K, *et al*. $CD4^+$ T cell-induced inflammatory cell death controls immune-evasive tumours. Nature. 2023; 618: 1033–1040.
[50] Speiser DE, Chijioke O, Schaeuble K, Münz C. $CD4^+$ T cells in cancer. Nature Cancer. 2023; 4: 317–329.
[51] Deng S, Vlatkovic T, Li M, Zhan T, Veldwijk MR, Herskind C. Targeting the DNA Damage Response and DNA Repair Pathways to Enhance Radiosensitivity in Colorectal Cancer. Cancers. 2022; 14: 4874.
[52] Qin C, Ji Z, Zhai E, Xu K, Zhang Y, Li Q, *et al*. PARP inhibitor olaparib enhances the efficacy of radiotherapy on XRCC2-deficient colorectal cancer cells. Cell Death & Disease. 2022; 13: 505.